

Low-cost LiMO₂ (M = Ni and Fe) Positive-Electrode Materials for Lithium Ion Batteries

Mohammed Adnan Mezaal^{1,2}, Limin Qu¹, Wei Liu¹, Guanghua Li¹, Xiaoyuan Zhao¹ and Lixu Lei^{1,*}

¹ School of Chemistry and Chemical Engineering, Southeast University, Nanjing, 211189, China.

² Department of Chemistry, College of Science, University of Karbala, Karbala, 56001, Iraq.

*E-mail: lixu.lei@seu.edu.cn

Received: 26 April 2016 / Accepted: 19 May 2016 / Published: 4 June 2016

Nickel-rich layered lithium transition-metal oxides, Li_{1.2}Ni_{1-x}M_xO₂ (M=transition metal), have been investigated intensively as high-energy cathode materials for lithium batteries because of their high specific capacity and relatively low-cost. However, oxygen loss from the lattice during the first charge and gradual structural transformation during cycling process can result in capacity fading and potential decay of the cathode materials, due to the fact that the highly oxidizing nature of tetravalent nickel. Herein, we report for the first time a series of promising and low-cost LiMO₂ (M = Ni and Fe) cathode materials for lithium ion batteries. We have successfully synthesized it by calcination of Ni₄Fe-layered double hydroxides (LDHs). The synthesized LDHs have been calcined in air or under oxygen flow for different period of time. Our results showed that it is possible to prepare low-cost with good electrochemical performance LiMO₂ from calcination of Ni₄Fe-LDHs at 750 °C for 12 h under flow of oxygen. The synthesized material showed excellent electrochemical performance with high capacity retention when cycled in the potential range of 2 to 4.5 V. It delivers a discharge capacity of 204 mAh/g at 20 mA/g and retains 85% of its capacity after 100 cycles.

Keywords: low-cost; cathode materials; lithium ion battery; layered double hydroxides

1. INTRODUCTION

One of the greatest challenges of this century is undeniably energy storage and conversion. The usage of energy from fossil fuels is a major contribution to the emission of greenhouse gases (GHGs), which has been rapidly increasing during the last decades leading to increasing concerns about climate alteration. Environment and energy issues forced us to search for an alternative source of energy. The alternative sources of energy like wind or solar energy are periodic and need sufficient energy storage device like battery to store the electricity in chemical form and use it when needed. Lithium ion battery is promising and has been intensively studied during last decade. LiCoO₂ is the most commonly used

positive electrode material in commercial secondary lithium batteries owing to its relatively high voltage, high reversible capacity and long cycle stability [1]. However, the toxicity and high cost of cobalt drive us to prepare low cost and environment friendly material for positive electrode of lithium ion batteries. Moreover, its energy density also need to be further improved. Thus, studies on substitution of Co by a low-cost elements, such as Mn and Ni, have been main concerns in recent years. One of the successful examples of LiMoO_2 layered-structure materials is $\text{Li}[\text{Ni}_{1/3}\text{Co}_{1/3}\text{Mn}_{1/3}]\text{O}_2$, which has already been commercialized for auto-mobile applications, since its cycling stability and safety characteristics are greater than that of LiCoO_2 [2]. However, cycling this material even at high potential of 4.5 V, it still deliver a low discharge capacity of 168 mAh/g which is quite low for use in next-generation EVs applications [3].

Nickel rich $\text{LiNi}_{1-x}\text{M}_x\text{O}_2$ ($\text{M} = \text{Co, Mn}$) ($1-x \geq 0.5$) are of great interest as potential positive electrode materials for high performances lithium ion batteries, since their high energy density, relatively low cost and environmental compatibility.[4, 5] Moreover, these materials can deliver higher discharge capacities and operate at higher potential of (4.4-4.8V) [5-7]than $\text{Li}[\text{Ni}_{1/3}\text{Co}_{1/3}\text{Mn}_{1/3}]\text{O}_2$, because the higher Ni content makes the main active redox species ($\text{Ni}^{2+} \leftrightarrow \text{Ni}^{4+}$) more in the layered structure. However, Ni-rich material suffers from the intrinsic thermal instability when it charges to a voltage higher than 4.4 V, results in poor cycle life and fast capacity fading which still plague their mass application. Moreover, due to the highly oxidizing nature of tetravalent nickel at highly delithiated state, Ni-rich materials is instable and can easily transform into spinel phase or into an electrochemically inactive NiO -like or with high volumetric changes, due to the loss of oxygen, and migration of nickel ions to the lithium site. The increased formation of NiO phase leads to capacity deteriorating. This instability of the delithiated phase can also results in safety issues [4, 5, 8-13]. Moreover, cycling the Ni-rich material at a temperature higher than 60 °C can catalyze the electrode-electrolyte side reactions, which forms a non-conducting solid electrolyte interface (SEI) layer that increases the diffusion path of Li^+ ion and declines the electrochemical performance of the material [14-16].

To synthesize a stable Ni-rich material, we have to fully understand its structure. Ni-rich materials are isostructural with LiNiO_2 layered hexagonal structure $\alpha\text{-NaFeO}_2$ space group R-3m.[17] The oxidation states of nickel, cobalt and manganese are typically divalent (Ni^{2+}), trivalent (Co^{3+}) and tetravalent (Mn^{4+}), in these structure [8, 18]. The Ni^{2+} and Co^{3+} ions are electrochemically active, while the Mn ions remaining as Mn^{4+} throughout the charge/discharge process. This tetravalent manganese provides substantial structural stability during electrochemical cycling even at the high voltage cutoff limit of 4.6 V, Myung *et al* reported [19, 20]. Furthermore, a considerable amount of Li and Ni is exchanged between the Li (3a site) and Ni/Co/Mn (3b site) layers due to the similar size of the Li^+ and Ni^{2+} . The impact of $\text{Li}^+/\text{Ni}^{2+}$ cation disordered distribution is considered one of the main reasons to induce the decrease in irreversible capacity and deterioration of the electrochemical performance. Intensive studies have been conducted to enhance the structural stability of Ni-rich materials and to decrease the $\text{Li}^+/\text{Ni}^{2+}$ cation disordering via surface coating or core shell structuring [7, 14, 21-28]. Moreover, it has been reported that Fe doping can significantly enhance the electrochemical performance of LiMO_2 material and improve its stability because it can expand the lattice c and reduce $\text{Ni}^{+2}/\text{Li}^+$ cation mixing [29]. Therefore, herein, we report $\text{LiNi}_{0.8}\text{Fe}_{0.2}\text{O}_2$ as cathode

materials for lithium ion batteries. The advantages of this material are as follow: it is easy to prepare; it has well-ordered structure with low $\text{Li}^+/\text{Ni}^{2+}$ cation mixing; Low-cost and shows an excellent electrochemical performance with good cycling stability.

2. EXPERIMENTAL SECTION

2.1. Syntheses of the materials

All chemicals used were of analytical grade without any further purification. $[\text{Ni}_4\text{Fe}(\text{OH})_{10}]\text{NO}_3$ was prepared by co-precipitation method as follow. A solution of 6.8 g $\text{LiOH}\cdot\text{H}_2\text{O}$ in distilled water was slowly dropped into a solution of 18.2 g $\text{Ni}(\text{NO}_3)_2\cdot 6\text{H}_2\text{O}$ and 6.1 g $\text{Fe}(\text{NO}_3)_3\cdot 9\text{H}_2\text{O}$ in 150 ml distilled water at 100 °C in an hour under flow of Ar and vigorous stirring. After the reaction mixture was stirred for another 10 h, it was filtered, washed and dried in vacuum at 50 °C. The precursor was homogeneously mixed with stoichiometric amount of LiOH inside glove box under argon, followed by heating at different conditions as follow: sample number one heated at 750 °C for 4 h in air; sample number two heated at 750 °C for 1 h under flow of O_2 gas; sample number three heated at 750 °C for 4 h under flow of O_2 gas and sample number four heated at 750 °C for 12 h under flow of O_2 gas. The furnace heating rate was maintained at $2\text{ }^\circ\text{C min}^{-1}$.

2.2. Physical characterization

Powder X-ray diffraction was performed on a Rigaku Ultima IV X-ray diffractometer with Cu K_α radiation. XRD data was collected at a scan rate of 0.2 degree min^{-1} with 0.02° step size in the 2θ range between 10° and 80°. The morphology of the materials was observed using a scanning electron microscope (SEM, FESEM Hitachi SU8010). Transmission electron microscopy (TEM) was performed on a JEM2000EX transmission electron microscope.

The electrode was prepared as follow: powder samples were mixed with acetylene carbon black (AB) and poly(vinylidene fluoride) (PVDF), mass ratio of 80 : 10 : 10, then dispersed in 1-methyl-2-pyrrolidinone (NMP). The slurry was spread onto a piece of aluminum foil, (a typical loading of the thin electrodes is about 3-4 mg cm^{-2}), and then dried in a vacuum oven at 65 °C for 24 h. CR 2032 coin cells were assembled in an Ar-filled glove box with Li metal as the counter electrode, 1 M LiPF_6 in ethylene carbonate and ethyl methyl carbonate, 1.0 M LiPF_6 in EC/EMC=50/50 (v/v), battery grade as the electrolyte (Sigma-Aldrich). The cells were galvanostatically charged/discharged within the range of 2 ~ 4.5 V at room temperature. The cells were galvanostatically charged at constant current to 4.5 V, followed by additional constant-voltage (CV) charging step at 4.5 V until the current reached 70% of the charge current and then discharged galvanostatically to 2 V using a battery cycler (Land battery testing system) at room temperature. The current densities used were 20, 100, 400, 1000 and 2000 mA g^{-1} . DSC measurements were carried out by heating the samples from 50 to 600 °C and the heating rate was maintained at $5\text{ }^\circ\text{C min}^{-1}$ under N_2 .

3. RESULTS AND DISCUSSION

3.1. Structure and morphology

The $[\text{Ni}_4\text{Fe}(\text{OH})_{10}]\text{NO}_3$ precursor was prepared by co-precipitation method as follow: A solution of 6.8 g $\text{LiOH}\cdot\text{H}_2\text{O}$ in distilled water was slowly dropped into a solution of 18.2 g $\text{Ni}(\text{NO}_3)_2\cdot 6\text{H}_2\text{O}$ and 6.1 g $\text{Fe}(\text{NO}_3)_3\cdot 9\text{H}_2\text{O}$ in 150 ml distilled water at 100 °C in an hour under vigorous stirring and N_2 flow, followed by aging for another 10 h. The precipitant was filtered, washed and dried in vacuum at 50 °C. The green powder was homogeneously mixed with stoichiometric amount of LiOH inside glove box under argon to avoid moisture, where mixing these two components outside the glove box leads to transformation of LiOH to Li_2CO_3 . After mixing the precursor with LiOH, the mixture was heated at different conditions as follow: sample number one heated at 750 °C for 4 h in air; sample number two heated at 750 °C for 1 h under flow of O_2 gas; sample number three heated at 750 °C for 4 h under flow of O_2 gas and sample number four heated at 750 °C for 12 h under flow of O_2 gas. The furnace ramp rate was maintained at 2 °C min⁻¹.

Layered double hydroxides (LDH) has a general formula of $[\text{M}^{2+}_{1-x}\text{M}^{3+}_x(\text{OH})]\text{A}^{n-} \cdot n\text{mH}_2\text{O}$, where M^{2+} and M^{3+} represent divalent and trivalent cations in the octahedral sites within the hydroxyl layers, x is equal to the ratio of $\text{M}^{3+}/(\text{M}^{2+} + \text{M}^{3+})$, typically in the range 0.17-0.33, and A^{n-} is the exchangeable interlayer anion, balancing the positive charge on the layers. The $\text{M}^{2+}/\text{M}^{3+}(\text{OH})_6$ octahedra form two-dimensional sheets that stack together by hydrogen bonding between the hydroxyl groups of adjacent sheets [30]. In this study, M^{2+} and M^{3+} represent Ni^{2+} and Fe^{3+} cations, respectively.

Figure 1 shows the XRD patterns of the synthesized samples. It can be seen that $[\text{Ni}_4\text{Fe}(\text{OH})_{10}]\text{NO}_3$ a typical crystalline layered double hydroxide (LDH) structure with a hexagonal stacking [31]. Heating the LDH material at 750 °C for 4 h in air results in cubic layered oxide (LDO) with space group Fm3m [32]. It is worth noting that heating this material in air could not form LiMO_2 layer, because in air Ni^{2+} cannot oxide to Ni^{3+} and therefore results in cubic structure Fm3m. The same phenomena has been observed during preparation of LiNiO_2 [33]. Therefore, we have calcined the LDH material under flow of oxygen at 750 °C for 1 h. As can be seen in Figure 1, the material calcined at 750 °C for 1 h under flow of oxygen exhibits a mixture of cubic Fm3m and layered R-3m structure. This is due to the fact that Ni^{2+} has been partially oxidized to Ni^{3+} and some intercalation of Li take place. This partial oxidation is due to the insufficient time, therefore, we have increased the calcination time to 4 h and the material displays layered structure with space group R-3m. However, some of the LiOH still not reacted and at this high temperature has been converted to Li_2CO_3 which is marked with a star as can be seen in Figure 1 [33]. To overcome this issue and to prepare pure phase layered structure R-3m, we have further increased the calcination time to 12 h, the material shows pure phase R-3m structure and the diffraction peaks of the XRD can be indexed based on the layered hexagonal structure ($\alpha\text{-NaFeO}_2$) type lattice space group (R-3m) [34-37].

The TG-DTG and DSC curves of the synthesized LDHs sample are shown in Figure 2 and 3, respectively. The mass losses of LDHs start at room temperature and ended at around 300 °C.

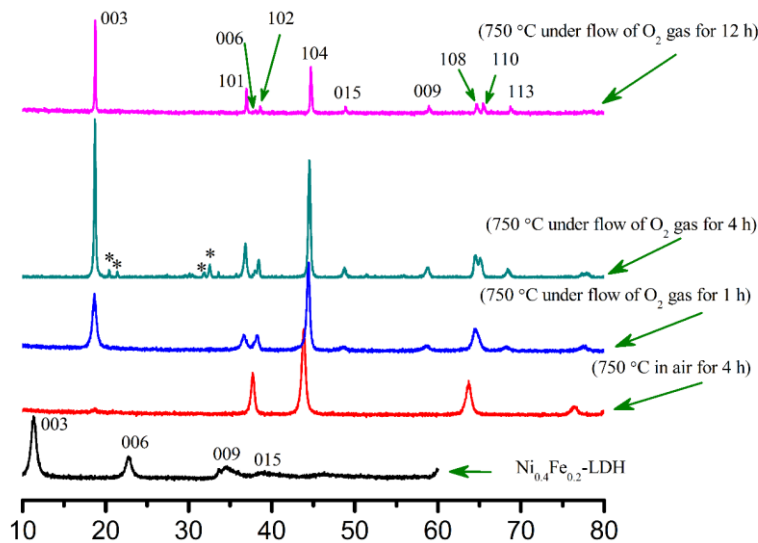


Figure 1. XRD patterns of the synthesized samples.

The 1st weight loss begins at room temperature and ends at around 190 °C, which corresponds to the loss of the adsorbed water and the interlayer water. The 2nd step ends at 300.0 °C which can be ascribed to the dehydroxylation and decomposition of the interlayer anions, which can be seen clearly in both of the DTG and DSC curves at 268 °C [38]. The dissociation peak appears at much lower temperature (268 °C) than earlier reported material, indicating that preparation of LiMO₂ from the precursor of LDHs is much easier than preparation from other precursor which is the advantage of our material [39]. For example, Balandeh *et al* reported that the decomposition of their prepared precursor appeared at 300 – 500 °C which indicates that synthesis of LiMO₂ from LDHs is much easier than reported material [39].

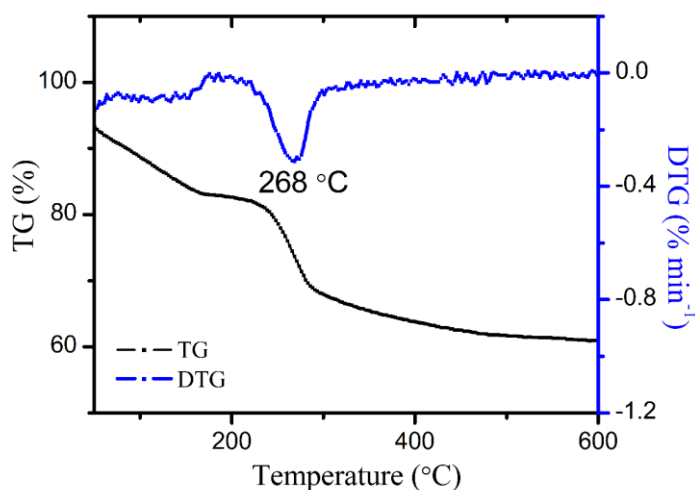


Figure 2. The TG/DTA curves of Ni4Fe-LDHs.

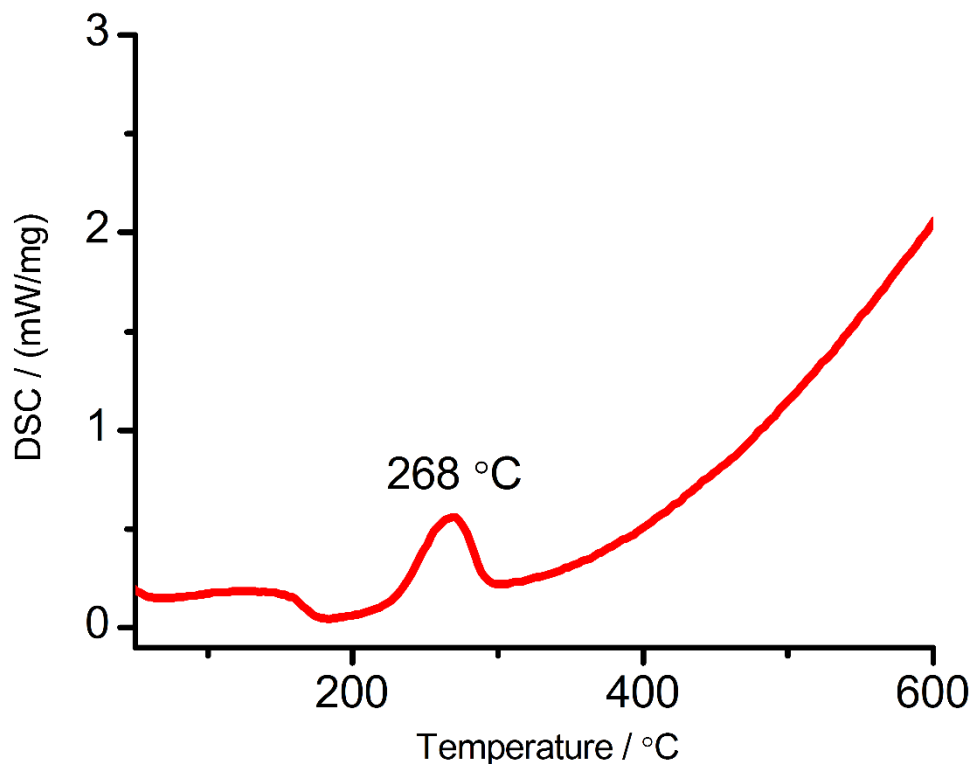


Figure 3. The DSC curve of Ni₄Fe-LDHs.

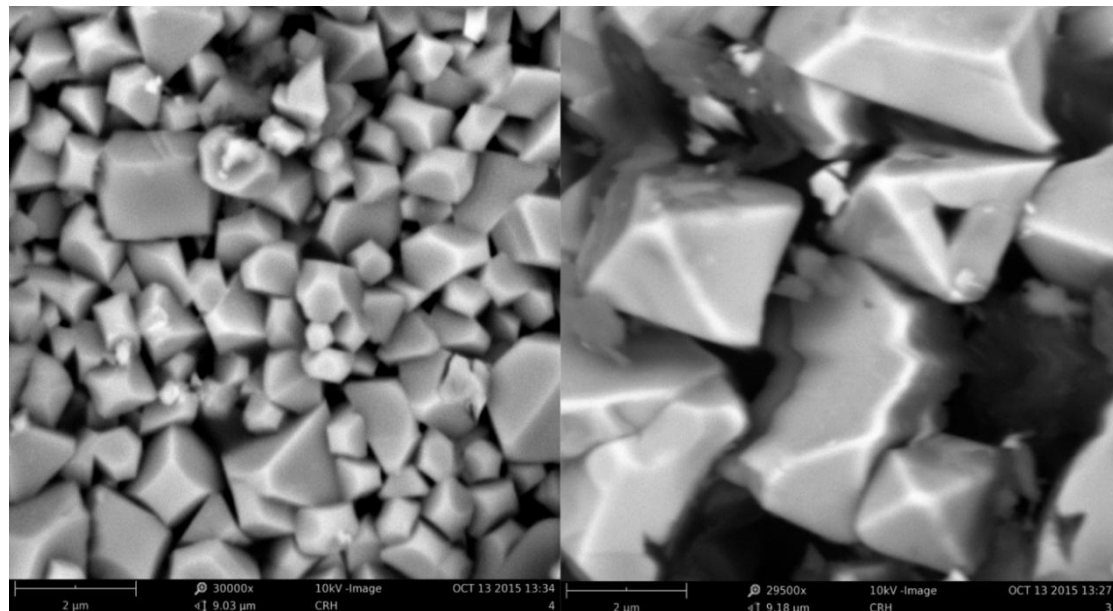


Figure 4. SEM images of LiNi_{0.8}Fe_{0.2}O₂ prepared at 700 °C under flow of oxygen for 12 h.

Figure 4 shows the SEM images of the samples. It displays regular and well-crystallized particles. To further characterize the synthesized material we have observed it with TEM as shown in Figure 5. It can be seen that the synthesized material at 750 °C possesses a primary particle with a

plate-like shape with dimensions around 100 nm and its selected area electron diffraction (SAED) pattern displays groups of lattice fringes with 0.248 nm, 0.145 nm and 0.125 nm interplanar spacing, which matches to the (101), (110), and (021) diffractions of the layered structure (α -NaFeO₂ type, space group R-3m), respectively [40]. This indicates that the synthesized material is a pure R-3m phase with no impurity observed.

3.2. Electrochemical performance

Figure 6 shows the first charge/discharge profiles of the synthesized samples. It can be seen that the material that synthesized at 750 °C for 4 h delivers lower discharge capacity than that of the 12 h. This is due to the presence of Li₂CO₃ on the surface of the material that calcined for 4 h only which blockage the diffusion channel for lithium ions and reduce its mobility, moreover, this material is not pure layered structure and has high Ni²⁺/Li⁺ cation mixing as calculated from the intensity peaks of the 003 and 104 planes and also according to c/a values that calculated from the XRD data as shown in Table 1, where the I_{003}/I_{104} and c/a values of the material the prepared at 750 °C for 12 h is higher than that of the material that prepared at 750 °C for 4 h indicating less cation mixing in the material that prepared for 12 h [41, 42]. As it is known that cation mixing occurs easily in LiMO₂ material (M = Ni) because the radius of Li⁺ (0.076 nm) is similar to that of Ni²⁺ (0.069 nm) which results in disordered structure and the higher value of I_{003}/I_{104} implies the lower cation mixing [43-45].

Table 1. Lattice parameters and intensity ratios of indicating peaks that calculated from XRD data.

Sample prepared at different temperature under flow of oxygen	a (Å)	c (Å)	c/a	I_{003}/I_{104}
750 C for 1h	2.86	13.89	4.85	0.768
750 C for 4h	2.862	14.00	4.89	1.164
750 C for 12h	2.861	14.293	4.99	1.390

The material that calcined for 4 h delivers an initial discharge capacity of 168 mAh/g, while the one that calcined for 12 h delivers a discharge capacity of 204 mAh/g at a current density of 20 mA/g. In comparison, the material that calcined for 12 h delivered much higher capacity and low-cost than earlier reported material by Chen *et al* [46], where their reported material delivered a discharge capacity of 146 mAh/g at 100 mA/g, while our synthesized material delivers a discharge capacity of ~202 mAh/g at 100 mA/g.

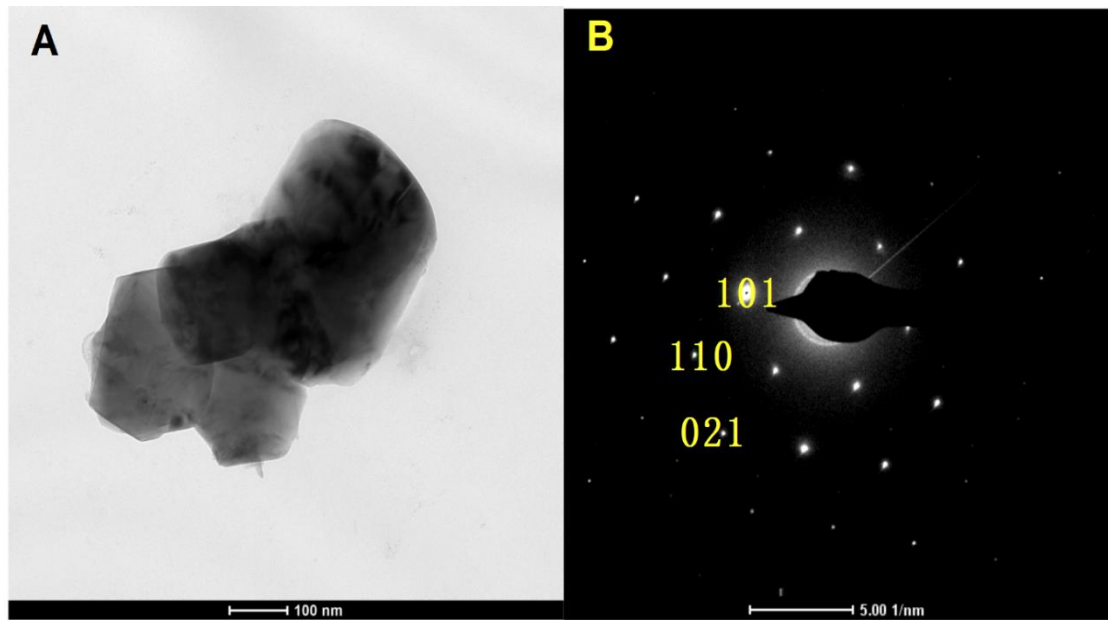


Figure 5. TEM images and electron diffraction pattern of $\text{LiNi}_{0.8}\text{Fe}_{0.2}\text{O}_2$ synthesized at 750 °C under flow of O_2 gas for 12 h.

To further investigate the synthesized material, we have cycled them at 20 mA/g for 100 cycles (Figure 7). The material that calcined at 750 °C for 12 h shows excellent capacity retention of 85 % after 100 cycles. While, the material that calcined for only 4 h shows fast capacity fading which could be ascribed to the high $\text{Ni}^{+2}/\text{Li}^+$ cation mixing and due to the presence of Li_2CO_3 which can blockage the diffusion path for Li ions and also reduced the electrochemically active material in the electrode.

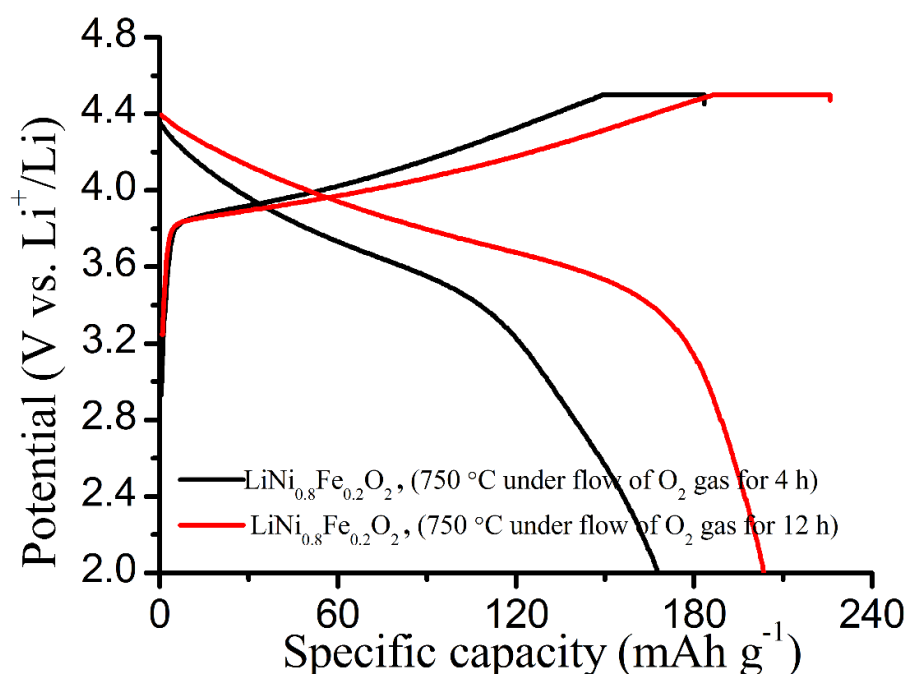


Figure 6. Initial charge-discharge profiles of the synthesized samples.

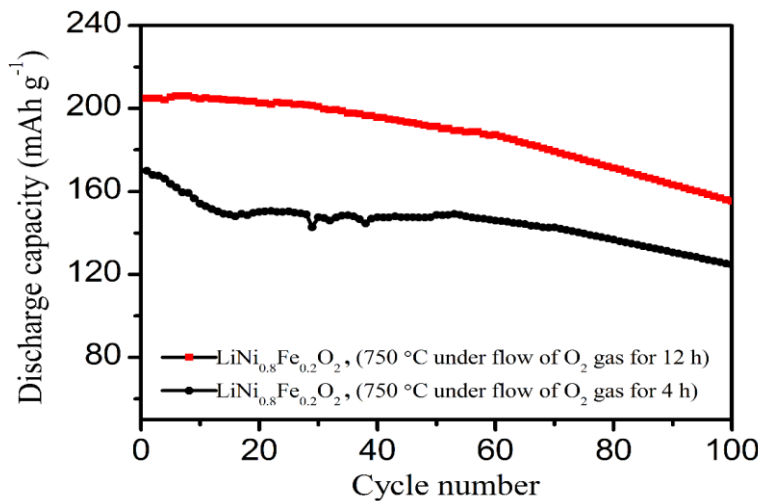


Figure 7. Cycling stability at 20 mA/g of the synthesized samples.

Rate capability test has been carried out at different current densities of 20, 100, 200, 400, 1000 and 2000 mA/g. It can be seen that the material that calcined for 12 h shows better electrochemical performance and higher discharge capacities at all rate because of it possesses single phase and well-ordered structure as shown in the XRD and TEM results (Figure 8).

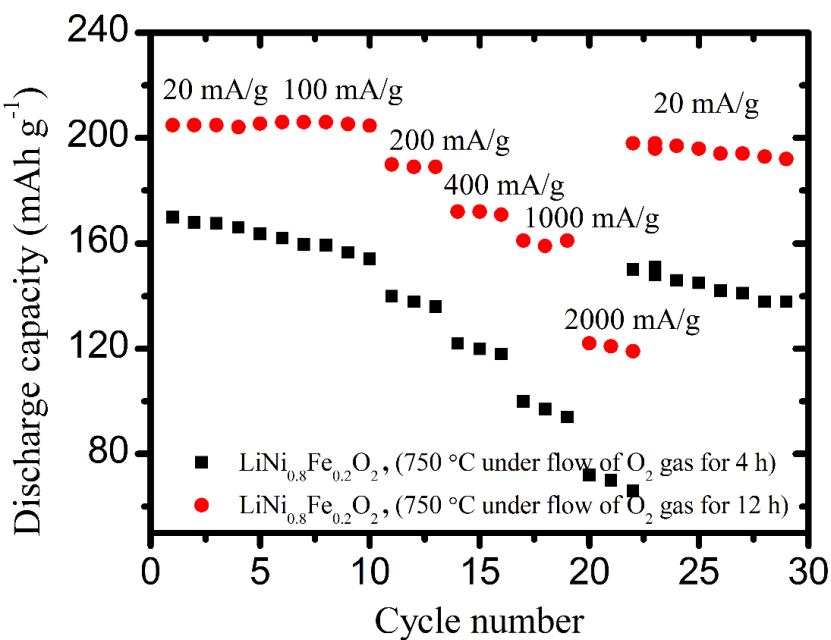


Figure 8. Rate capabilities of the synthesized materials at different current densities.

This material reported here can be easily prepared with low-cost, shows an excellent electrochemical performance and much better stability and retained higher capacity than earlier reported material. For example, Li *et al* [47] reported LiNi_{0.8}Co_{0.1}Mn_{0.1}O₂ cathode materials, our

synthesized material is cheaper because it has no cobalt. Furthermore, their synthesized material was cycled between 2.7 and 4.3 V and delivered a discharge capacity of 192.4 mAh g^{-1} at a current density of 18 mA g^{-1} , and the capacity retention after 40 cycles is 91.56%. While, our synthesized material delivers a 204 mAh/g at a current density of 20 mA/g and retained 85 % of its capacity after 100 cycles when cycled between 2 and 4.5 V as shown in Figure 8. This indicates that our synthesized material is more stable than the earlier reported material even when cycled to higher upper cut-off potential.

4. CONCLUSIONS

In this study, a series of Ni₄Fe-LDHs have been successfully synthesized by coprecipitation method. The synthesized LDHs have been calcined in air or under oxygen flow for different time. Our results showed that it is possible to prepare low-cost with good electrochemical performance LiMO₂ (M = Ni and Fe) cathode materials for lithium ion batteries from calcination of Ni₄Fe-LDHs at 750 °C for 12 h under flow of oxygen. The synthesized material showed excellent electrochemical performance with high retention capacity when cycled in the potential range of 2 to 4.5 V.

References

1. T. Wei, R. Zeng, Y. Sun, Y. Huang, K. Huang, *Chem Commun (Camb)*, 50 (2014) 1962-1964.
2. J. Wilcox, S.b. Patoux, M. Doeff, *Journal of The Electrochemical Society*, 156 (2009) A192.
3. M.H. Lee, Y.J. Kang, S.T. Myung, Y.K. Sun, *Electrochimica Acta*, 50 (2004) 939-948.
4. V. Augustyn, S. Therese, T.C. Turner, A. Manthiram, *J. Mater. Chem. A*, 3 (2015) 16604-16612.
5. Y.K. Sun, Z. Chen, H.J. Noh, D.J. Lee, H.G. Jung, Y. Ren, S. Wang, C.S. Yoon, S.T. Myung, K. Amine, *Nat Mater*, 11 (2012) 942-947.
6. L. Zhang, N. Li, B. Wu, H. Xu, L. Wang, X.Q. Yang, F. Wu, *Nano Lett*, 15 (2015) 656-661.
7. F. Wu, N. Li, Y. Su, L. Zhang, L. Bao, J. Wang, L. Chen, Y. Zheng, L. Dai, J. Peng, S. Chen, *Nano Lett*, 14 (2014) 3550-3555.
8. Y.K. Sun, S.T. Myung, M.H. Kim, J. Prakash, K. Amine, *J Am Chem Soc*, 127 (2005) 13411-13418.
9. X. Yang, D. Wang, R. Yu, Y. Bai, H. Shu, L. Ge, H. Guo, Q. Wei, L. Liu, X. Wang, *Journal of Materials Chemistry A*, 2 (2014) 3899.
10. H.-H. Sun, W. Choi, J.K. Lee, I.-H. Oh, H.-G. Jung, *Journal of Power Sources*, 275 (2015) 877-883.
11. A.R. Armstrong, N. Dupre, A.J. Paterson, C.P. Grey, P.G. Bruce, *Chemistry of Materials*, 16 (2004) 3106-3118.
12. A.R. Armstrong, M. Holzapfel, P. Novak, C.S. Johnson, S.H. Kang, M.M. Thackeray, P.G. Bruce, *J Am Chem Soc*, 128 (2006) 8694-8698.
13. D. Mohanty, J. Li, D.P. Abraham, A. Huq, E.A. Payzant, D.L. Wood, C. Daniel, *Chemistry of Materials*, 26 (2014) 6272-6280.
14. Y. Cho, P. Oh, J. Cho, *Nano Lett*, 13 (2013) 1145-1152.
15. J. Xu, Y. Hu, T. liu, X. Wu, *Nano Energy*, 5 (2014) 67-73.
16. N.-S. Choi, J.-G. Han, S.-Y. Ha, I. Park, C.-K. Back, *RSC Adv.*, 5 (2015) 2732-2748.
17. J. Zheng, W.H. Kan, A. Manthiram, *ACS Appl Mater Interfaces*, 7 (2015) 6926-6934.
18. B.R. Long, J.R. Croy, F. Dogan, M.R. Suchomel, B. Key, J. Wen, D.J. Miller, M.M. Thackeray, M. Balasubramanian, *Chemistry of Materials*, 26 (2014) 3565-3572.

19. W.-S. Yoon, Y. Paik, X.-Q. Yang, M. Balasubramanian, J. McBreen, C.P. Grey, *Electrochemical and Solid-State Letters*, 5 (2002) A263.
20. S.-T. Myung, S. Komaba, K. Hosoya, N. Hirosaki, Y. Miura, N. Kumagai, *Chemistry of Materials*, 17 (2005) 2427-2435.
21. J. Lu, Q. Peng, W. Wang, C. Nan, L. Li, Y. Li, *J Am Chem Soc*, 135 (2013) 1649-1652.
22. Y.K. Sun, M.J. Lee, C.S. Yoon, J. Hassoun, K. Amine, B. Scrosati, *Adv Mater*, 24 (2012) 1192-1196.
23. C. Li, H.P. Zhang, L.J. Fu, H. Liu, Y.P. Wu, E. Ram, R. Holze, H.Q. Wu, *Electrochimica Acta*, 51 (2006) 3872-3883.
24. K.X. Wang, X.H. Li, J.S. Chen, *Adv Mater*, 27 (2015) 527-545.
25. R. Guo, P. Shi, X. Cheng, L. Sun, *Electrochimica Acta*, 54 (2009) 5796-5803.
26. Z. Zheng, Z.-G. Wu, Y.-J. Zhong, C.-H. Shen, W.-B. Hua, B.-B. Xu, C. Yu, B.-H. Zhong, X.-D. Guo, *RSC Adv.*, 5 (2015) 37330-37339.
27. P. Hou, X. Wang, D. Wang, D. Song, X. Shi, L. Zhang, J. Guo, J. Zhang, *RSC Advances*, 4 (2014) 15923.
28. Q. Xie, Z. Hu, C. Zhao, S. Zhang, K. Liu, *RSC Adv.*, 5 (2015) 50859-50864.
29. W. El Mofid, S. Ivanov, A. Konkin, A. Bund, *Journal of Power Sources*, 268 (2014) 414-422.
30. W. Shen, Y. Wang, X. Shi, N. Shah, F. Huggins, S. Bollineni, M. Seehra, G. Huffman, *Energy & Fuels*, 21 (2007) 3520-3529.
31. M. Hu, L. Lei, *Journal of Solid State Electrochemistry*, 11 (2006) 847-852.
32. B. Wang, B.C. Chakoumakos, B.C. Sales, J.B. Bates, *Journal of Solid State Chemistry*, 122 (1996) 376-383.
33. W. Li, J. Reimers, J. Dahn, *Physical Review B*, 46 (1992) 3236-3246.
34. J.-H. Park, J.-H. Cho, S.-B. Kim, W.-S. Kim, S.-Y. Lee, S.-Y. Lee, *Journal of Materials Chemistry*, 22 (2012) 12574.
35. H. Liu, C. Chen, C. Du, X. He, G. Yin, B. Song, P. Zuo, X. Cheng, Y. Ma, Y. Gao, *J. Mater. Chem. A*, 3 (2015) 2634-2641.
36. X. Li, H. Xin, Y. Liu, D. Li, X. Yuan, X. Qin, *RSC Adv.*, 5 (2015) 45351-45358.
37. Y. Huang, X. Hou, S. Ma, X. Zou, Y. Wu, S. Hu, Z. Shao, X. Liu, *RSC Adv.*, 5 (2015) 25258-25265.
38. Q. Tao, Y. Zhang, X. Zhang, P. Yuan, H. He, *Journal of Solid State Chemistry*, 179 (2006) 708-715.
39. M. Balandeh, S. Asgari, *Journal of Nanomaterials*, 2010 (2010) 1-6.
40. C. Yang, Q. Zhang, W. Ding, J. Zang, M. Lei, M. Zheng, Q. Dong, *J. Mater. Chem. A*, 3 (2015) 7554-7559.
41. M.A. Mezaal, L. Qu, G. Li, R. Zhang, J. Xuejiao, K. Zhang, W. Liu, L. Lei, *RSC Adv.*, 5 (2015) 93048-93056.
42. H.-J. Noh, S. Youn, C.S. Yoon, Y.-K. Sun, *Journal of Power Sources*, 233 (2013) 121-130.
43. C. Gong, W. Lv, L. Qu, O.E. Bankole, G. Li, R. Zhang, M. Hu, L. Lei, *Journal of Power Sources*, 247 (2014) 151-155.
44. E. Han, Q. Jing, L. Zhu, G. Zhang, S. Ma, *Journal of Alloys and Compounds*, 618 (2015) 629-634.
45. L.-W. Liang, K. Du, Z.-D. Peng, Y.-B. Cao, G.-R. Hu, *Chinese Chemical Letters*, 25 (2014) 883-886.
46. H. Li, G. Chen, B. Zhang, J. Xu, *Solid State Communications*, 146 (2008) 115-120.
47. L.-j. Li, X.-h. Li, Z.-x. Wang, H.-j. Guo, P. Yue, W. Chen, L. Wu, *Powder Technology*, 206 (2011) 353-357.